# Effects of Wall Roughness, Impeller Blades and Diffuser Vanes on the Performances of a First Stage Centrifugal Pump

Nicolas La Roche-Carrier, Guyh Dituba Ngoma and Walid Ghie

*University of Quebec in Abitibi-Témiscamingue, School of Engineering 445,*
*Boulevard de l'Université, Rouyn-Noranda, Quebec, J9X 5E4, Canada*

Abstract:     In this study, the first stage of a multistage centrifugal pump was numerically investigated to improve its design. The continuity and Navier-Stokes equations with the k-ε turbulence model and standard wall functions were used. The effects of the wall roughness height, impeller blade height and diffuser vane height, and the number of diffuser vanes on the performances of the first pump stage were analyzed. The results achieved demonstrate that the selected parameters affect the pump stage head, brake horsepower and efficiency in a strong yet different manner. To validate the approach developed, the results of the numerical simulations were compared with the experimental results.

## 1 INTRODUCTION

Multistage centrifugal pumps are widely used in industrial and mining enterprises. One of the most important components of a multistage centrifugal pump is the impeller (Peng, 2008). For a more performing multistage pump, its design parameters must be determined accurately. Given the three-dimensional and turbulent liquid flow in a multistage centrifugal pump, it is very important to be aware of the liquid flow's behavior when flowing through a pump stage accounting for the wall roughness. This can be achieved by taking all stage components into consideration in the planning, design and optimization phases in design and off-design conditions.

Many experimental and numerical studies have been conducted on the liquid flow through a multistage centrifugal pump. A three-dimensional turbulent flow through an entire stage of a multistage centrifugal pump was numerically simulated using a CFD code (Huang et al., 2006), including flows in a rotating impeller and stationary diffuser. It was found that the reverse flows existed near the impeller outlet, resulting in the flow field being asymmetric and unstable. Moreover, the impacts of the return vane profile on the performances of the multistage centrifugal pump

were experimentally investigated to optimize the stationary components in the multistage centrifugal pump (Miyano et al., 2008). It was found, among other things, that the return vane, whose trailing edge was set at the outer wall radius of the downstream annular channel and discharged the swirl-less flow, had a positive impact on pump performances, while the effects of the diffuser vane on the performances of the multistage centrifugal pump were experimentally investigated (Kawashima et al., 2008), accounting for the interactions among the diffuser vane, return vane and next stage impeller. The relevance in matching the diffuser vane and return vane properly to improve the pump efficiency of the multistage centrifugal pump was shown. In addition, the multistage pump problems in conjunction with the axial thrust were experimentally examined (Gantar et al., 2002), the Laser Doppler Anemometry (LDA) was used to determine the fluid rotation in the impeller side chamber and its impact on the impeller hydraulic axial thrust for different leakage flow regimes.

Deepened analysis of previous studies clearly demonstrated that the research results obtained are specific to the design parameters and configuration of the rotating and stationary components in multistage centrifugal pumps, and thus cannot always be generalized. Therefore, in this study, to improve the design and performances of multistage

centrifugal pumps, accounting for the particularities of the geometry and configuration of the impeller and diffuser with return vanes, a numerical investigation was conducted using the ANSYS-CFX code (Ansys inc., 2011) based on the finite volume method and Rhie Chow algorithm for the pressure-velocity coupling. This was done to gain further insight into the characteristics of the three-dimensional turbulent liquid flow through a stage of a multistage centrifugal pump while also considering various flow conditions, the height of the wall roughness, the heights of the impeller blade and diffuser vane, and the number of diffuser vanes. Moreover, the pump stage head, brake horsepower and efficiency were represented as a function of the flow rate in order to identify the values of selected design parameters that might enhance pump stage performances with respect to their value ranges.

## 2 GOVERNING EQUATIONS

Fig. 1 shows the model of the first stage of a multistage centrifugal pump considered in this study. It consists of an impeller, diffuser with return vanes and casting.
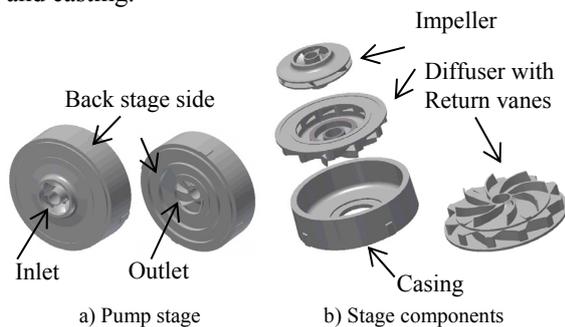


Figure 1: Model of a centrifugal pump stage.

To run the numerical simulations, the used domain fluids of the impeller and diffuser with return vanes are shown in Fig. 2.
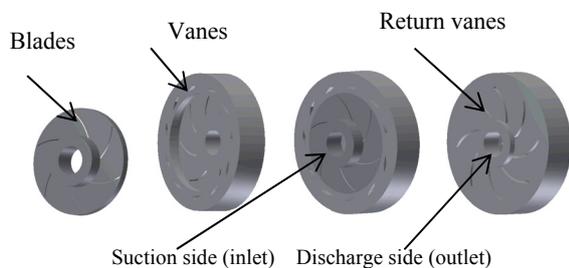


Figure 2: Domain fluids of impeller, diffuser and pump stage.

In the centrifugal pump stage's governing equations for liquid flow, the following assumptions were made: (i) a steady state, three-dimensional and turbulence flow using the k-ε model was assumed; (ii) it was an incompressible liquid; (iii) it was a Newtonian liquid; and (iv) the liquid's thermophysical properties were constant with the temperature (density, viscosity, etc.).

To account for these assumptions, the theoretical analysis of the liquid flow in the impeller passages, diffuser vane passages and diffuser return vane passages was based on the continuity and Navier-Stokes equations (Tropea et al., 2007). For the three-dimensional liquid flow through these components of a centrifugal pump stage as shown in Fig. 2, the continuity equations are expressed by:

$$\nabla \cdot \vec{V}_{vel} = 0 , \tag{1}$$

where $\vec{V}_{vel} = \vec{V}_{vel}\left(u(x,y,z), v(x,y,z), w(x,y,z)\right)$ is the liquid flow velocity vector.

Using the coordinate system, Eq. 1 can be rewritten as:

$$\frac{\partial u}{\partial x} + \frac{\partial v}{\partial y} + \frac{\partial w}{\partial z} = 0 \tag{2}$$

and the Navier–Stokes equations are given by:

$$\rho \nabla \cdot (\vec{V}_{vel} \otimes \vec{V}_{vel}) = \mu_{eff} \nabla \cdot (\nabla \vec{V}_{vel} + (\nabla \vec{V}_{vel})^T) - \nabla p + B \tag{3}$$

where p is the pressure, ρ is the density, $\mu_{eff}$ is the effective viscosity accounting for turbulence, $\otimes$ is a tensor product and B is the source term, which is equal to zero for the flow in the stationary components like the diffuser.

For flows in an impeller rotating at a constant speed ω, the source term can be written as follows:

$$B = -\rho\left(2\vec{\omega}x\vec{V}_{vel} + \vec{\omega}x(\vec{\omega}x\vec{r})\right) \tag{4}$$

where $\vec{r}$ is the location vector, $2\vec{\omega}x\vec{V}_{vel}$ is the centripetal acceleration and $\vec{\omega}x(\vec{\omega}x\vec{r})$ is the Coriolis acceleration.

Using the coordinate system, Eq. 3 can be rewritten as:

$$\rho\left(u\frac{\partial u}{\partial x}+v\frac{\partial u}{\partial y}+w\frac{\partial u}{\partial z}\right)=\mu_{eff}\left(\frac{\partial^2 u}{\partial x^2}+\frac{\partial^2 u}{\partial y^2}+\right.$$
$$\left.\frac{\partial^2 u}{\partial z^2}\right)-\frac{\partial p}{\partial x}+B_x$$
$$\rho\left(u\frac{\partial v}{\partial x}+v\frac{\partial v}{\partial y}+w\frac{\partial v}{\partial z}\right)=\mu_{eff}\left(\frac{\partial^2 v}{\partial x^2}+\frac{\partial^2 v}{\partial y^2}+\right.$$
$$\left.\frac{\partial^2 v}{\partial z^2}\right)-\frac{\partial p}{\partial y}+B_y \qquad (5)$$
$$\rho\left(u\frac{\partial w}{\partial x}+v\frac{\partial w}{\partial y}+w\frac{\partial w}{\partial z}\right)=\mu_{eff}\left(\frac{\partial^2 w}{\partial x^2}+\frac{\partial^2 w}{\partial y^2}+\right.$$
$$\left.\frac{\partial^2 w}{\partial z^2}\right)-\frac{\partial p}{\partial z}+B_z$$

where

$B_x=\rho\left(\omega_z^2 r_x+2\omega_z v\right)$, $B_y=\rho\left(\omega_z^2 r_y-2\omega_z u\right)$ and $B_z=0$.
Furthermore, $\mu_{eff}$ is defined as $\mu_{eff}=\mu+\mu_t$, where $\mu$ is the dynamic viscosity and $\mu_t$ is the turbulence viscosity, it is linked to turbulence kinetic energy k and dissipation ε via the relationship: $\mu_t=C_\mu\rho k^2\varepsilon^{-1}$ where $C_\mu$ is a constant.

The values for k and ε stem directly from the differential transport equations for turbulence kinetic energy and turbulence dissipation rates:

$$\nabla.(\rho\vec{V}_{vel}k)=\nabla.[(\mu+\frac{\mu_t}{\sigma_k})\nabla k]+p_k-\rho\varepsilon \qquad (6)$$

$$\nabla.(\rho\vec{V}_{vel}\varepsilon)=\nabla.[(\mu+\frac{\mu_t}{\sigma_\varepsilon})\nabla\varepsilon]+\frac{\varepsilon}{k}(C_{\varepsilon 1}p_k-C_{\varepsilon 2}\rho\varepsilon) \qquad (7)$$

where $C_{\varepsilon 1}$, $C_{\varepsilon 2}$ and $\sigma_\varepsilon$ are constants. $p_k$ is the turbulence production due to viscous and buoyancy forces, which is modeled using:

$$p_k=\mu_t\nabla\vec{V}_{vel}.(\nabla\vec{V}_{vel}+\nabla\vec{V}_{vel}^T)+p_{kb}$$
$$-\frac{2}{3}\nabla.\vec{V}_{vel}(3\mu_t\nabla.\vec{V}_{vel}+\rho k) \qquad (8)$$

$$p_{kb}=-\frac{\mu_t}{\rho\sigma_\rho}g.\nabla\rho \qquad (9)$$

where $p_{kb}$ can be neglected for the k-ε turbulence model.

Additionally, for the flow modeling near the wall, the logarithmic wall function is used to model the viscous sub-layer (Tropea et al., 2007).

To solve equations 2 and 5 numerically while accounting for the boundary conditions and turbulence model k-ε, the ANSYS-CFX code. In the cases examined involving the pump stage, the boundary conditions were formulated as follows: the static pressure provided was given at the stage inlet, while the flow rate provided was specified at the stage outlet. The frozen rotor condition was used for the impeller-diffuser interface. A no-slip condition was set for the flow at the wall boundaries.

The pump stage head is determined as follows:

$$H=\frac{p_{to}-p_{ti}}{\rho g} \qquad (10)$$

where $p_{ti}$ is the total pressure at the pump stage inlet and $p_{to}$ the total pressure at the pump stage outlet as shown in Fig. 2. They are expressed as:

$$p_{ti}=p_i+\frac{\rho}{2}V_{vel_i}^2 \quad \text{and} \quad p_{to}=p_o+\frac{\rho}{2}V_{vel_o}^2 \qquad (11)$$

Moreover, the hydraulic power of the pump stage is given by $P_h=\rho QgH$, where Q is the flow rate and H is the pump stage head.

In addition, the brake horsepower of the pump stage is expressed as $P_s=C\omega$, where ω is the angular velocity and C is the impeller torque.

From the hydraulic power and the brake horsepower, the efficiency of the pump stage can be written as $\eta=\frac{P_h}{P_s}$. It can also be formulated in terms of the hydraulic efficiency ($\eta_h$), the volumetric efficiencies ($\eta_v$), and mechanical efficiency ($\eta_m$) as $\eta=\eta_h\eta_v\eta_m$.

## 3 RESULTS AND DISCUSSION

Water at 25 °C was used as the working liquid for all simulation runs in this study. The main reference data used for the impeller were 195 mm for the inner diameter, 406 mm for the outer diameter, 6 for the number of blades and 1750 rpm for the rotating speed. For the diffuser, the main reference data were 407.016 mm for the inner diameter, 571.5 mm for the outer diameter, 11 for the number of vanes and 8 for the number of return vanes. The numerical simulation results presented in this work were obtained with the highest accuracy by conducting mesh-independent solution tests in each case study using different numbers of mesh elements.

### 3.1 Impact of Wall Roughness Height

To analyze the impact of the wall roughness height of the impeller, diffuser and casting on the pump stage performances, two wall roughness heights (0 mm, and 2 mm) were chosen, while the other

parameters were kept constant. Fig. 3 shows the head as a function of the flow rate, where it is observed that the head is not affected by the value of the wall roughness height at 0 mm. On the contrary, it decreases when the wall roughness height increases further. This is explained by the fact that the friction loss rises with significantly increasing wall roughness height. In other words, the wall roughness increases the flow resistance in turbulent flow. As shown in Fig. 4, the brake horsepower rises with increasing wall roughness height for large flow rates due to the increase in the friction loss with increasing wall roughness height for large flow rates. Thus, the requested pump torque increases.
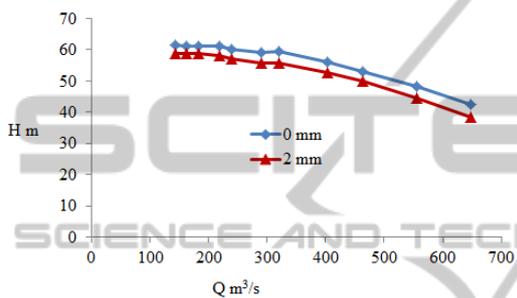


Figure 3: Pump stage head versus flow rate.
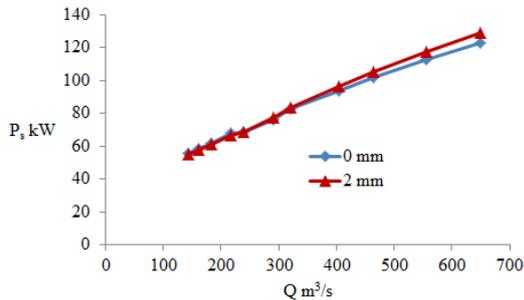


Figure 4: Brake horsepower versus flow rate.

In addition, Fig. 5 shows the efficiency as a function of the flow rate, where it is observed that the efficiency decreases with increasing wall roughness height due to the increase in friction loss.
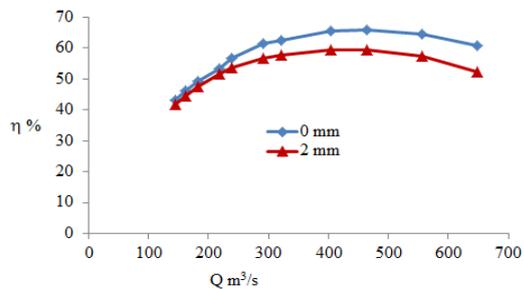


Figure 5: Efficiency versus flow rate.

Moreover, Fig. 6 shows the corresponding static pressure contour for $Q = 464$ m$^3$/h, which demonstrates the distribution of static pressure in the impeller and diffuser with return vanes. Also, Tab. 1 presents the pressure differences in the impeller, diffuser and diffuser return vane passages obtained for the wall roughness heights of 0 mm and 2 mm. There, the decrease in total pressure difference with increasing wall roughness height is shown.



Diffuser return vane passages
a) 0 mm and $\Delta p = 519683$ Pa



Diffuser return vane passages
b) 2 mm and $\Delta p = 486555$ Pa
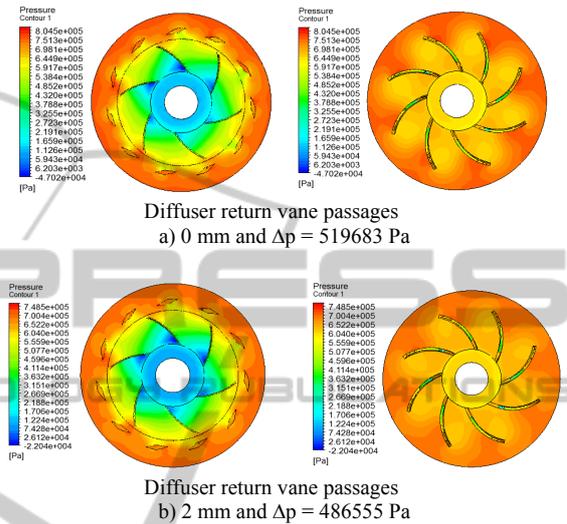
Figure 6: Static pressure contour.

Table 1: Distribution of pressure difference.

| Wall rough. height mm | Pressure difference $\Delta p$ | | | Pa |
| --- | --- | --- | --- | --- |
| | Impeller | Diffuser | Diffuser return vane passages | $\Delta p_{total}$ |
| 0 | 512751 | 108942 | -102010 | 519683 |
| 2 | 486786 | 79951 | -80182 | 486555 |

## 3.2 Impact of the Height of Impeller Blades and Diffuser Vanes

To investigate the impact of the height of impeller blades and diffuser vanes on the pump stage performances, the values of 16 mm, 23 mm and 29 mm were selected for the impeller blade height and diffuser vane height, while keeping the other parameters constant. Fig. 7 shows that the pump stage head decreases with increasing flow rate due to decreasing liquid pressure. In addition, the pump stage head increases with increasing blade height and vane height. This is explained by the fact that when the flow rate is kept constant, the increased blade height leads to the decreasing meridional velocity, which increases the pump stage head since

the outlet tangential velocity and outlet blade angle remain constant. In other words, the liquid pressure drops in the impeller and the diffuser decreases as a function of the increase in the blade height and vane height.
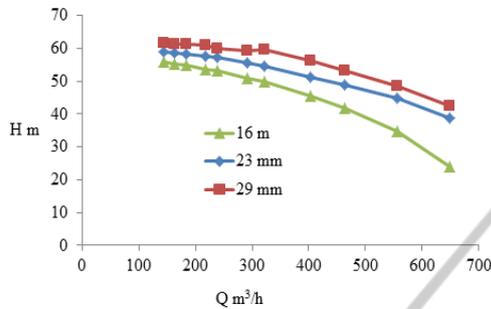


Figure 7: Pump stage head versus flow rate.

Furthermore, the curves expressing the pump stage brake horsepower as a function of the flow rate are shown in Fig. 8, illustrating that the brake horsepower increases with increasing flow rate. This is explained by the additional decrease in liquid pressure relative to the flow rate. Also, the brake horsepower increases relative to the impeller blade height due to the requested increase in pump shaft torque relative to the increased blade height.
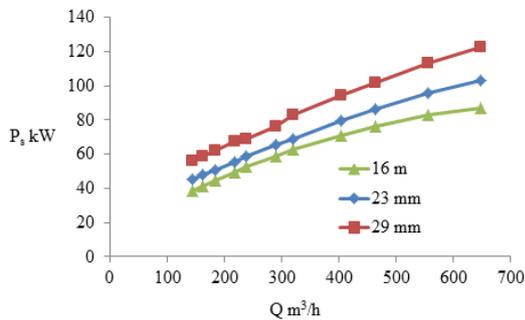


Figure 8: Brake horsepower versus flow rate.
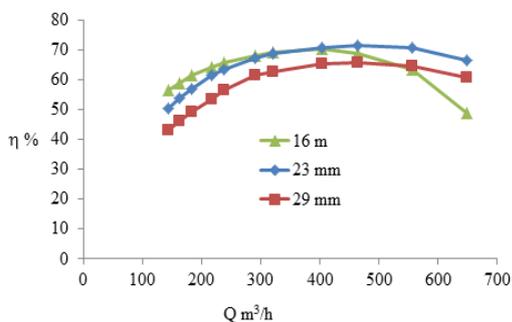


Figure 9: Efficiency versus flow rate.

In addition, Fig. 9 shows that the efficiency for the

blade height and vane height of 16 mm decreases rapidly to the right of the BEP. The efficiency of the blade height and vane height of 23 mm is highest at large flow rates, whereas the efficiency of the blade height and vane height of 29 mm is lowest at flow rates ranging between 150 $m^3$/h and 550 $m^3$/h.

Figs. 10 and 11 represent the corresponding contours for static pressure and liquid flow velocity vectors for Q = 464 $m^3$/h. Fig. 10 clearly shows that the static pressure increases with increasing blade height and vane height. This is due mainly to the decrease in liquid flow velocity at the impeller outlet as depicted in Fig. 11, where the average liquid flow velocities at the impeller outlet decrease from 18.43 for 16 mm to 15.67 m/s for 29 mm. Also, the recirculation phenomenon is observed in the diffuser return vane passages. Furthermore, the distribution of pressure difference ($\Delta p = p_o - p_i$) in the stage components is presented in Tab. 2.

Table 2: Distribution of the pressure difference.

| Blade or vane height mm | Pressure difference $\Delta p$ Pa | | | |
|---|---|---|---|---|
| | Impeller | Diffuser | Diffuser return vane passages | $\Delta p_{total}$ |
| 16 | 424908 | 74626 | -91742 | 407792 |
| 23 | 485468 | 92713 | -98754 | 479427 |
| 29 | 512751 | 108942 | -102010 | 519683 |



Diffuser return vane passages
a) Height = 16 mm and $\Delta p = 407792$ Pa



Diffuser return vane passages
b) Height = 23 mm and $\Delta p = 479427$ Pa



Diffuser return vane passages
c) Height = 29 mm and $\Delta p = 519683$ Pa
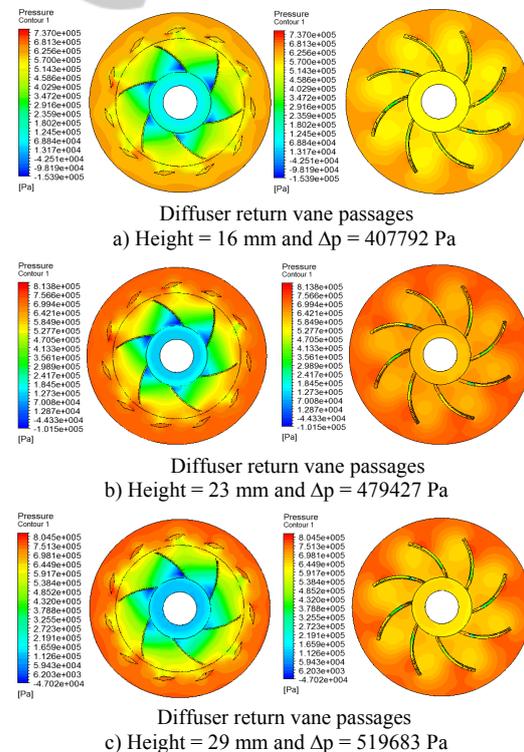
Figure 10: Static pressure contour.

Diffuser return vane passages
a) Height = 16 mm



Diffuser return vane passages
b) Height = 23 mm



Diffuser return vane passages
c) Height = 29 mm
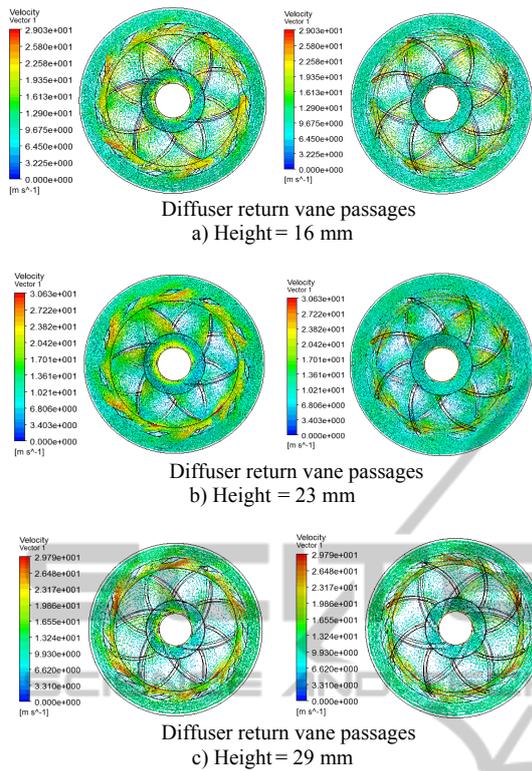
Figure 11: Liquid flow velocity vector.

## 3.3 Impact of the Number of Diffuser Vanes

To examine the impact that the number of diffuser vanes has on the pump stage head, brake horsepower and efficiency, three diffuser models (with 7, 8 and 12 vanes, and 8 return vanes) were selected considering an impeller with 5 blades, while other parameters were kept constant. Fig. 12 shows the head as a function of the flow rate, where it is observed that the head obtained with diffusers with 7 and 8 vanes is almost the same for a flow rate smaller than 320 m$^3$/h, whereas the head with the diffuser with 12 vanes is smallest. For large flow rates, the head with the diffuser with 12 vanes is the highest. This is due to a rise in static pressure through the reduction in flow velocity in a diffuser. The flow guidance and friction effect depend on the number of diffuser vanes, and the flow rate. When the number of diffuser vanes increases, the diffuser vane passages become narrower. This leads to better fluid guidance. In other words, flow loss decreases as the number of diffuser vanes increases. Friction loss increases with an increasing number of diffuser vanes. Furthermore, flow guidance, friction loss and static pressure conversion are affected by the flow rate. Thus, there is an antagonistic impact between

the diffusion impact and the friction loss in the range of the flow rate considered. As depicted in Fig. 13, brake horsepower variation due to the number of diffuser blades is also small, even if the lowest brake horsepower is reached with 12 diffuser blades.
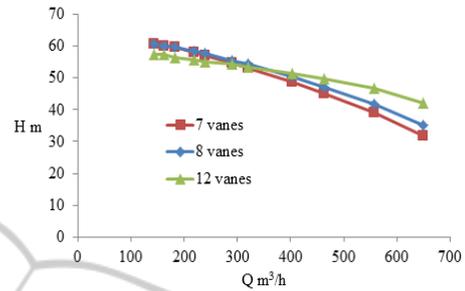


Figure 12: Pump stage head versus flow rate.
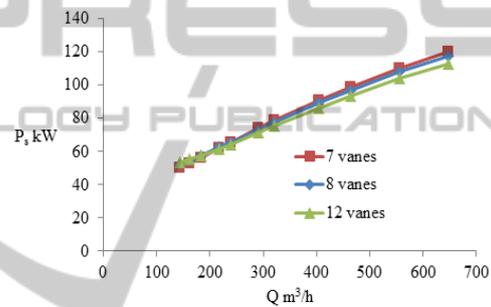


Figure 13: Brake horsepower versus flow rate.

In addition, Fig. 14 shows that for low and high flow rates, the efficiency of 12 diffuser vanes is highest whereas the efficiency for 7 and 8 diffuser vanes is nearly the same for a flow rate smaller than 320 m$^3$/h. This figure also indicates that the efficiency is lowest for 7 diffuser vanes for a flow rate higher than 320 m$^3$/h. Moreover, the BEP moves towards large flow rates and rises as the number of diffuser vanes increases.
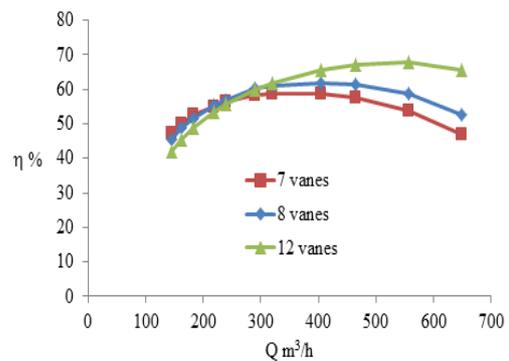


Figure 14: Efficiency versus flow rate.

Furthermore, Figs. 15 and 16 show the corresponding static pressure contour and liquid flow velocity vector for Q = 403 m³/s, respectively, illustrating that for these figures, there is a correlation between increased static pressure difference and decreased liquid flow velocity at the diffuser outlet, with an increased diffuser vane number. The average liquid flow velocity values at the diffuser outlet of 13.94 m/s, 13.14 m/s and 11 m/s were found for 7, 8 and 12 vanes respectively, as shown in Fig. 16. Also, Tab. 3 indicates the pressure difference in the impeller, diffuser and diffuser return vane passages.



| a) 7 vanes | b) 8 vanes | c) 12 vanes |
| ΔP = 482224 Pa | ΔP = 498668 Pa | ΔP = 500843 Pa |
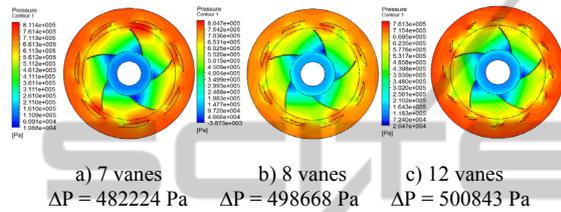
Figure 15: Static pressure contour.



a) 7 vanes    b) 8 vanes    c) 12 vanes
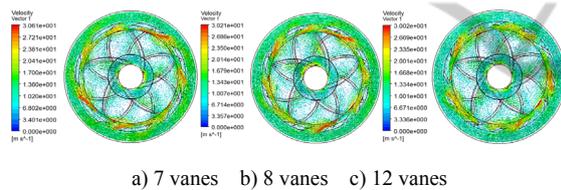
Figure 16: Vectors of liquid flow velocity.

Table 3: Distribution of pressure difference.

| Vane | Pressure difference Δp  Pa | | | |
| | Impeller | Diffuser | Diffuser return vane passages | $\Delta p_{total}$ |
|---|---|---|---|---|
| 7 | 5 10556 | 70817 | -89149 | 482224 |
| 8 | 496559 | 87279 | -85170 | 498668 |
| 12 | 476198 | 103252 | -78607 | 500843 |

## 3.4 Model Comparison

To validate the model developed for the first pump stage, the numerical simulation results were compared with the experimental results (Technosub inc.), as shown in Fig. 17, where it is observed that all the numerical curves for the head, brake horsepower and efficiency follow the trend of the experimental curves; however, additional parameters, which affect the gap between the numerical results and experimental results are being more thoroughly investigated in the experimental and numerical sides to increasingly enhance the approach developed for the first pump stage.
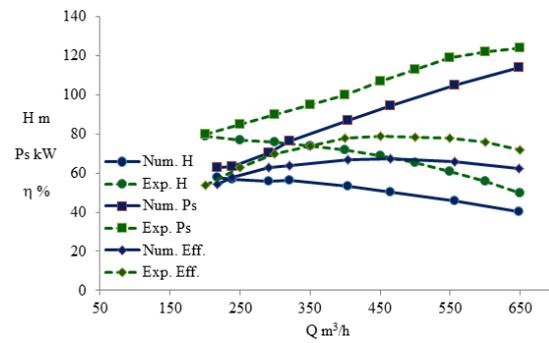


Figure 17: Comparison between the numerical and experimental results.

## 4 CONCLUSIONS

In this work, a liquid flow in the first stage of a multistage centrifugal pump was numerically examined. A model of a first pump stage was developed to analyze the impacts of the wall roughness height; the height of the impeller blades and diffuser vanes, and the number of diffuser vanes on the pump stage performances. The results achieved reveal, among other things, that higher wall roughness heights of the impeller and diffuser negatively affect the pump stage head, brake horsepower and efficiency; the pump stage head and brake horsepower increase as the height of the impeller blades and diffuser vanes increases. Moreover, the pump stage head and efficiency rise for large flow rates with increasing numbers of diffuser vanes, whereas the brake horsepower hardly varies at all regardless of the number of diffuser vanes. In all, the numerical curves obtained for the head, brake horsepower and efficiency well follow the trend of the experimental results.

## NOMENCLATURE

B     source term (Nm⁻³)
C     torque (Nm)
g     acceleration of gravity (ms⁻²)
H     head (m)
P     power (W)
p     pressure (Nm⁻²)
$p_\kappa$   turbulence production due to viscous and buoyancy forces
Q     flow rate (m³s⁻¹)
r     radial coordinate (m)
V     velocity (ms⁻¹)
u     flow velocity in x direction (ms⁻¹)

v      flow velocity in y direction ($\text{ms}^{-1}$)
w      flow velocity in z direction ($\text{ms}^{-1}$)
x      x-coordinate (m)
y      y-coordinate (m)
z      z-coordinate (m)

**Greek symbols**

$\Delta$      difference
$\varepsilon$      turbulence dissipation ($\text{m}^2\ \text{s}^{-3}$),
$\eta$      efficiency
$\kappa$      turbulence kinetic energy ($\text{kg m}^{-2}\ \text{s}^{-2}$)
$\rho$      fluid density ($\text{kg m}^{-3}$)
$\mu$      dynamic viscosity (Pa s)
$\mu_{eff}$      effective viscosity (Pa s)
$\mu_t$      turbulence viscosity (Pa s)
$\Omega$      angular velocity ($\text{rad s}^{-1}$)

**Subscripts**

1      inlet
2      outlet
h      hydraulic
i      inlet
m      mechanical
o      outlet
s      shaft
t      total
v      volumetric
vel      velocity

# ACKNOWLEDGEMENTS

# REFERENCES

Peng W., 2008. *Fundamentals of turbomachinery*. Hoboken, New Jersey, John Wiley and Sons.

Huang S., Islam M.F., Liu P., 2006. Numerical simulation of 3 D turbulent flow through an entire stage in a multistage centrifugal pump. *International Journal of Computational Fluid Dynamics,* Vol. 20, Issue 5, Pages 309-314.

Miyano M., Kanemoto T., Kawashima D., Wada A., Hara T., Sakoda K., 2008. Return Vane Installed in Multistage Centrifugal Pump. *International Journal of Fluid Machinery and Systems* Vol. 1, No. 1.

Kawashima D., Kanemoto T., Sakoda K., Wada A., Hara T., 2008. Matching Diffuser Vane with Return Vane Installed in Multistage Centrifugal Pump. *International Journal of Fluid Machinery and Systems*, Vol. 1, No. 1.

Gantar M., Florjancic D., and Sirok B., 2002. Hydraulic Axial Thrust in Multistage Pumps - Origins and Solutions. *Journal Fluids Engineering*, Vol. 124, Issue 2, 336-341.

Ansys inc., 2011. *ANSYS-CFX (CFX Introduction, CFX Reference Guide, CFX Tutorials, CFX-Pre User's Guide, CFX-Solver Manager User's Guide, CFX-Solver Modeling Guide, CFX-Solver Theory Guide)*, release 14.0, USA.

Tropea C., Yarin A. L., Foss J. F., 2007. *Handbook of experimental fluid mechanics*. Springer-Verlag, Berlin, Heidelberg.

Technosub Inc., www.technosub.net.